TATION PAGE

Form Approved
OBM No. 0704-0188

1. Agency Use Only *(Leave blank).*	2. Report Date. June 1993	3. Report Type and Dates Covered. Final - Journal Article

4. Title and Subtitle.
On the validity of the wedge assemblage method for pressure-release sinusoids

5. Funding Numbers.
Program Element No. 0601153N
Project No. 3202
Task No. 350
Accession No. DN257115
Work Unit No. 571506003

6. Author(s).
Richard S. Keiffer

7. Performing Organization Name(s) and Address(es).
Naval Research Laboratory
Acoustic Simulation and Tactics Branch
Stennis Space Center, MS 39529-5004

8. Performing Organization Report Number.
NRL/JA/7181--92-0001

9. Sponsoring/Monitoring Agency Name(s) and Address(es).
Naval Research Laboratory
Center for Environmental Acoustics
Stennis Space Center, MS 39529-5004

10. Sponsoring/Monitoring Agency Report Number.
NRL/JA/7181--92-0001

11. Supplementary Notes.
Published in J. Acoust. Soc. Am.

12a. Distribution/Availability Statement.
Approved for public release; distribution is unlimited.

12b. Distribution Code.

13. Abstract *(Maximum 200 words).*

In the past, the wedge assemblage (WA) method for calculating the acoustic scattering from rough, long-crested, or corrugated surfaces has been compared with both experimental data and exact theory with good results. Nevertheless, significant questions about what physics is included in the method and its realm of validity remain unanswered. In this paper, the WA method is applied to scattering from pressure-release sinusoidal surfaces in order to further explore these topics. Comparisons with accurate benchmark calculations are carried out over a broad range of kh and $k\Lambda$ (k is the acoustic wave number; h and Λ are the amplitude and wavelength of the sinusoid, respectively) indicate that the primary limitation of the WA method stems from its current failure to include multiple scattering effects. It is also shown that quite good agreement with the benchmark can be achieved by a "diffraction-only" WA model even when $kh \ll 1$ and "reflectionlike" scattering patterns are observed.

14. Subject Terms.
Acoustic scattering, reverberation, surface roughness

15. Number of Pages. 11

16. Price Code.

17. Security Classification of Report.	18. Security Classification of This Page.	19. Security Classification of Abstract.	20. Limitation of Abstract.
Unclassified	Unclassified	Unclassified	SAR

On the validity of the wedge assemblage method for pressure-release sinusoids

Richard S. Keiffer
Naval Research Laboratory, Stennis Space Center, Mississippi 39529-5004

(Received 25 October 1992; accepted for publication 8 February 1993)

In the past, the wedge assemblage (WA) method for calculating the acoustic scattering from rough, long-crested, or corrugated surfaces has been compared with both experimental data and exact theory with good results. Nevertheless, significant questions about what physics is included in the method and its realm of validity remain unanswered. In this paper, the WA method is applied to scattering from pressure-release sinusoidal surfaces in order to further explore these topics. Comparisons with accurate benchmark calculations are carried out over a broad range of kh and $k\Lambda$ (k is the acoustic wave number; h and Λ are the amplitude and wavelength of the sinusoid, respectively) indicate that the primary limitation of the WA method stems from its current failure to include multiple scattering effects. It is also shown that quite good agreement with the benchmark can be achieved by a "diffraction-only" WA model even when $kh \ll 1$ and "reflectionlike" scattering patterns are observed.

PACS numbers: 43.30.Hw, 43.20.Fn

INTRODUCTION

Although the basic principles involved in the wedge assemblage method (WA) have been confirmed in a number of experimental and numerical studies,[1-7] several questions regarding the validity of the method and the physics included in it remain unanswered. For example, there has been some general interest in the validity of the WA approach for smooth surfaces (i.e., decidedly unwedgelike surfaces) as a function of scattering geometry, frequency, surface shape, etc. In particular, questions have been raised regarding the behavior of the model when the surface roughness get very small compared to an acoustic wavelength (λ). To address this particular question, it is necessary to gain a deeper understanding of the roles that reflections and diffractions play in WA modeling. Other questions that have been raised concern the sensitivity of the WA calculations to the particular assemblage being used. Finally, the WA approach employed here is a true single-scatter model. In the analysis of the accuracy of the WA model this limitation must be taken into account.

The present study aims at examining these issues and beginning to examine others by considering the problem of scattering from pressure-release sinusoidal surfaces. The approach taken is to probe for the limitations of the WA method, as it applies to plane-wave scattering, through comparisons with benchmark results. By observing the behavior of the WA model vice the benchmark over a range of kh and $k\Lambda$ (where k is the acoustic wave number; h and Λ are the surface amplitude and wavelength, respectively) and scattering geometries, it is hoped that some conclusions might be drawn about what physics it (the WA model) includes. In the process of completing this benchmarking exercise, it is also shown that the WA model lends new physical insight to this already thoroughly examined problem.

I. THE BENCHMARK PROBLEM AND SOLUTION TECHNIQUE

In many of the recent papers in which approximate scattering methods have been investigated, the primary tools for analysis have been accurate numerical solutions to an exact theory. In this study, this approach has been adopted by using a formulation of the method of moments (MOM) to solve for the scattered field and its normal derivative on a pressure-release sinusoidal surface (and hence for the far-field scattering) that results from an incident plane wave. Complete details of this approach are not presented here as there are several good descriptions in the published papers.[8-10] Essentially, the formulation that Thorsos[10] gives for solving the appropriate Fredholm integral equation of the first kind has been implemented. There are, however, several points concerning details of the calculations that should be mentioned.

First, consider the scattering geometry: a sinusoidal surface of length L and mean height zero is insonified from above and from the left by a plane-wave source that is incident at an angle θ_{inc}. The corrugations of the sinusoid are parallel to the y axis as is the distant line source that generates the incident plane wave. The angle θ_{inc} is measured from the $-x$ axis to $-\mathbf{k}_{\text{inc}}$ (the incident wave vector). A line receiver is located far from the sinusoid in the θ_{scat} direction, measured from the $-x$ axis to $\mathbf{k}_{\text{scat}}$ (the scattered wave vector). Here, R_S and R_R are the distances from the center of the scattering patch to the source and receiver, respectively. The scattering geometry is shown in Fig. 1.

As is typically done when dealing with scattering surfaces of finite extent, the magnitude of incident field is tapered in order to minimize any strong diffractions from the edges of the scattering surface. Reference 10 goes into some detail on this subject and derives a complex taper function which, provided $kg \sin\theta_{\text{inc}} \gg 1$, satisfies the wave equation to order $1/(kg \sin\theta_{\text{inc}})^2$ (g controls the tapering

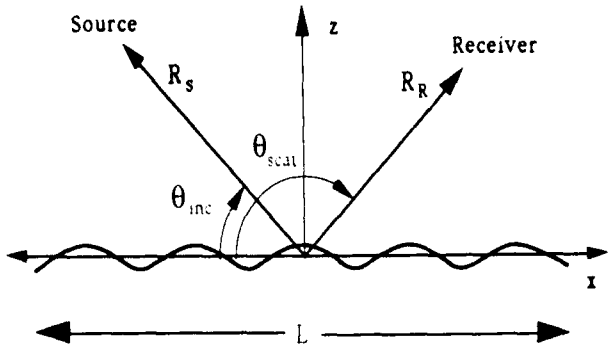

FIG. 1. Scattering geometry for benchmark problem.

rate). Through numerical experimentation (not shown here but supplied in the review process), it has been determined that for the cases studied in this paper a simplified version of this incident or source field:

$$P_{inc}(x,z)=P_0 D(x,z)\exp[ik(x\cos\theta_{inc}+z\sin\theta_{inc})], \tag{1}$$

where

$$D(x,z)=\exp[-(x-z\cot\theta_{inc})^2/g^2] \tag{2}$$

yielded essentially the same results. This apparent compromise of the stated goal to perform *benchmark* comparisons has no significant numerical effects and allows for the convenience of using the same insonification function for the WA calculations. Most importantly, none of the conclusions drawn from the benchmark comparisons are in any way altered by this substitution. In Eq. (1), a point on the scattering surface is specified by the ordered pair (x,z). As for the taper parameter g, a value of $g=L/4$ (where L is total length of the sinusoid) was found acceptable in Thorsos' study and is adopted here as well. Except where noted otherwise, all sinusoids studied were sampled at a rate of $\Delta x=\lambda/10$ for the MOM calculations.

The quantity that will be compared in the benchmark tests is the scattering strength:

$$\mathrm{SS}=10\times\log\sigma(\theta_{inc},\theta_{scat}). \tag{3}$$

Here, $\sigma(\theta_{inc},\theta_{scat})$ is the dimensionless scattering cross section per unit angle per unit surface length.[10,11] Assuming a time harmonic, plane wave source, a distant receiver, and a 1-D surface, $\sigma(\theta_{inc},\theta_{scat})$ is given by

$$\sigma(\theta_{inc},\theta_{scat})=R_R I_{scat}/LI_{inc}, \tag{4}$$

where I_{scat}, I_{inc} are the magnitudes of the scattered and incident acoustic intensities, respectively. Under the conditions stated, this scattering problem is two dimensional so the pressure has units of force per unit length [as does P_0 in Eq. (1)] and the acoustic intensity has units of energy per unit time per unit length. If the incident plane wave field is tapered as in Eq. (1), an average incident intensity is usually defined,

$$I_{inc}=\Pi_{inc}/L\sin(\theta_{inc}), \tag{5}$$

where Π_{inc} is the instantaneous power radiated through the length of surface. For a source described by Eq. (1),

$$\Pi_{inc}=\frac{P_0^2}{\eta c}\int_{-\infty}^{\infty}[D(x,z)]^2\frac{\mathbf{k}_{inc}(-\hat{z})}{|\mathbf{k}_{inc}|}dx=\frac{gP_0^2\sin\theta_{inc}}{\eta c}\sqrt{\frac{\pi}{2}}. \tag{6}$$

Here, η is the density (mass/area) of the 2-D fluid and c is the sound speed. Now, the dimensionless cross section can be written as

$$\sigma(\theta_{inc},\theta_{scat})=\frac{\eta c R_R I_{scat}}{gP_0^2\sqrt{\pi/2}}. \tag{7}$$

A scattering strength based on the cross section defined in Eq. (7) and calculated from the scattered field predicted by the MOM model, serves as the benchmark or reference against which the WA calculations are compared.

II. THE WA METHOD FOR SMOOTH 1-D SURFACES

A. Background/general remarks

The wedge assemblage (WA) method is a time domain technique developed to describe the scattering of acoustic fields from arbitrarily rough surfaces in terms of a particular theory for acoustic scattering from a wedge. Usually, the method involves only single scattering although in principle multiple scattering can be included. Like its frequency domain counterpart, the facet-ensemble method,[3] the technique was originally developed for point sources and 1-D surfaces.[7] More recently, based on heuristic arguments and experimental evidence,[1] it has been extended to 2-D surfaces.[12] The building block of the original as well as the extended method is an exact, analytic, time domain solution formulated by Biot and Tolstoy (BT) for the acoustic impulse response of an infinite, acoustically hard wedge.[13] The corresponding solution for the pressure-release wedge was developed later[3] and differs from the hard wedge solution only slightly.

Following Medwin,[1] the original BT solution can be modified so as to appear in a more convenient form. This is accomplished by assuming a point source that consists of a uniform and instantaneous volume flow at time $t=0$. With this source, the radiated pressure pulse at range R takes on the form of an impulse: $(\rho S/4\pi R)\delta(t-R/c)$, where S has units (volume/time) and ρ is the density. The BT solution for the scattered pressure field consists of two time-separable parts:

$$P(t)=P_{ref}(t)+P_\delta(t). \tag{8}$$

Of the two distinct terms, the first to arrive at the receiver, if the particular scattering geometry permits, are any reflections (P_{ref}). These are delta functions in time. Next to arrive is the diffracted pressure wave (P_δ) that radiates from the wedge apex:

$$P_\delta(t)=\left(\frac{-S\rho c}{4\pi\theta_w}\right)\{\beta\}[rr_0\sinh(Y)]^{-1}\exp\left(\frac{-\pi Y}{\theta_w}\right), \tag{9}$$

where

$$\beta=\frac{\sin[(\pi/\theta_w)(\pi\pm\theta\pm\theta_0)]}{1-2\exp(-\pi Y/\theta_w)\cos[(\pi/\theta_w)(\pi\pm\theta\pm\theta_0)]+\exp(-2\pi Y/\theta_w)} \tag{10}$$

and

$$Y=\cosh^{-1}\left(\frac{c^2t^2-(r^2+r_0^2+Z^2)}{2rr_0}\right). \tag{11}$$

The diffracted component of the solution arrives at the receiver at a time (τ_0) that corresponds to the shortest source to apex to receiver path:

$$\tau_0=\frac{[(r+r_0)^2+Z^2]^{1/2}}{c}. \tag{12}$$

Here, Z is the offset distance along the wedge apex between source and receiver (which is zero for this study), r_0, θ_0 and r, θ are the source and receiver coordinates respectively; θ_w is the wedge angle. Note that θ_0 and θ are angles measured in the surrounding fluid from a single face of the wedge. The term $(\pi\pm\theta\pm\theta_0)$ is written for simplicity. For the hard wedge, the curly bracket term $\{\beta\}$ consists of the sum of the four terms obtained by using the four possible combination of angles, $\pm\theta$ and $\pm\theta_0$. For the pressure-release wedge, change the sign of $\sin(\pi+\theta+\theta_0)$ and $\sin(\pi-\theta-\theta_0)$ before summing. The geometry used by the BT solution is shown in Fig. 2. This exact solution applies to arbitrarily located point sources and receivers, and all wedge angles.

The WA method begins with the discretization of the deterministic surface of interest. For long-crested or corrugated surfaces, it is easy to visualize rectangular facets (long axis parallel to the surface corrugations) fit to the surface. At intersections between two facet faces, a long wedge apex is defined. In this way, the surface of interest is converted to an assemblage of truncated wedges having infinitely long apexes. The key to the WA method is to apply the physical insight that the BT solution provides for the perfect wedge problem to a new but related problem.

In previous applications of the WA method to rough surface scattering problems, the emphasis has been on the term in the BT solution that represents the diffracted wave. The somewhat curious fact is that for published WA studies involving rough surfaces, the term in the BT solution that corresponds to a reflection from a wedge face has played a nearly nonexistent role. It should be emphasized that in this study, it was not necessary to include any facet reflections in order to achieve good results. Indeed, an inspection of the benchmark results and the physics of the BT solution suggests that it would be incorrect to include this term for the scattering problem considered. From the numerical experiment that follows, it will be shown that one reason that facet reflections can successfully be ignored in this study is that in a certain limiting case the diffracted wave behaves like the impulsive image reflection.

B. The diffracted wave in WA modeling

In order to apply the BT solution for the apex-diffracted wave to the assemblage of wedges, one ignores the fact that the assemblage is composed of wedges defined by finite-width facets. One imagines a new BT geometry centered on the apex of each of the truncated wedges. Basically, this approximation means that the diffracted wave that reaches the receiver depends only on the incident field near the apex, the wedge angle, and the scattering direction. One can understand this approximation for the apex-diffracted wave to be within the single-scatter approximation. In the WA method, the BT solution for the diffracted wave is applied to each member of the wedge assemblage and summed with due respect to time of arrival.

It may be observed from Eqs. (9)–(12) that when the diffracted first arrives ($t=\tau_0$), the BT solution is singular due to the behavior of $\sinh(Y)$. In numerical modeling it is often desirable to calculate the impulse response at discrete time intervals so that a fast Fourier transform (FFT) can be performed. This suggests that the average of the diffracted wave over a unit time interval be used to numerically handle this singularity. In this paper, a numerical integration via a Romberg technique is used to calculate the mean value of the diffracted field over a unit time interval. For further details, see Ref. 2.

Since it will help to explain the results obtained for the benchmark comparisons, it is convenient at this time to

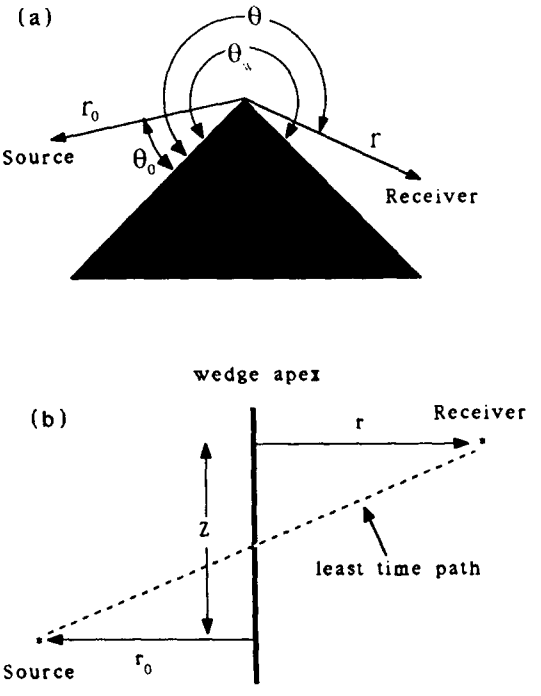

FIG. 2. Geometry for Biot–Tolstoy solution: (a) side view, (b) top view.

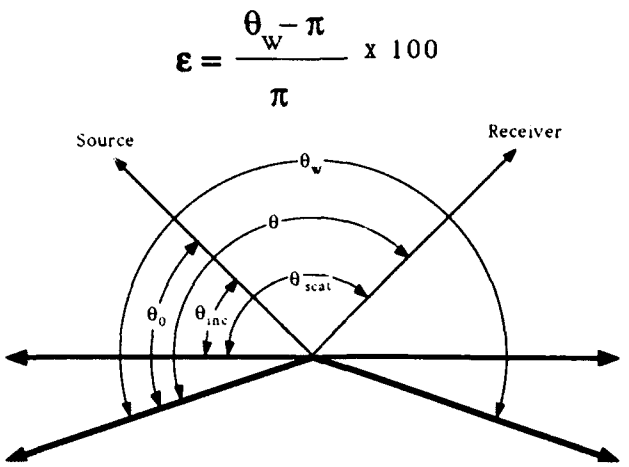

FIG. 3. Geometry for the analysis of diffraction from an almost flat wedge.

point out that under certain circumstances, the diffracted wave can behave very much like a reflection. That is, the time series for the diffracted wave becomes indistinguishable from the impulsive image solution. To see how this can occur, consider an arbitrarily located point source and receiver above an infinite flat surface having either Dirichlet (pressure-release) or Neumann (hard) boundary conditions. The method of images gives the solution for any source/receiver combination. Tracing the shortest ray from the source to a point on the flat surface to the receiver identifies the so-called specular point. If the source is impulsive (a delta function in time) then the time of flight for the received reflection (also a delta function) clearly corresponds to this ray path.

Now, replace the flat surface by an infinite wedge whose apex is located at the specular point. Begin the numerical experiment with the wedge angle (θ_w) slightly greater than π and let θ_w slowly approach π (see Fig. 3). When $\theta_w = \pi$, the diffractive term of the BT solution is zero (as it is for θ_w equal to any integral submultiple of π). As θ_w approaches π, the diffraction disappears precisely at the point that the image reflection moves into the direction of the receiver. The fact that the total field is continuous through this transition implies that the diffracted wave must approach the response of the impulsive reflection as the wedge angle shrinks to π.

This behavior of the diffracted wave is illustrated in Fig. 4 which shows the time and frequency response of the diffract wave relative to the image reflected wave for several different values of θ_w. The family of curves that depend on wedge angle are expressed as the percentage that θ_w differs from π. For this experiment, θ_{inc} was 45 deg and θ_{scat} was 135 deg; both were held fixed. Note that as θ_w gets closer to π, θ_0 gets closer to θ_{inc}, θ gets closer to θ_{scat} and the diffracted wave becomes very much like a delta function. The response has the correct sign and the strength of the image reflected wave in the either domain.

From this experiment, one can say that in a numerical sense it does not matter if the return from the specular point is due to a reflection from a flat surface or a diffraction from a very slightly wedged surface. One can understand from this result that the reflection from an infinite flat plane can be regarded as the limiting case of diffraction from the apex of an infinite wedge. Further, it suggests that for surfaces such as sinusoids, where there are no flat patches of finite area (the local radius of curvature is never infinite), a diffraction-only model is arguably more consistent than one in which reflections from flat patches are included. Later in this paper, it will be shown that for a finite length sinusoidal surface whose roughness is quite small compared to an acoustic wavelength, diffractions of this kind describe the expected reflectionlike scattering pattern, i.e., the incident beam pattern is observed.

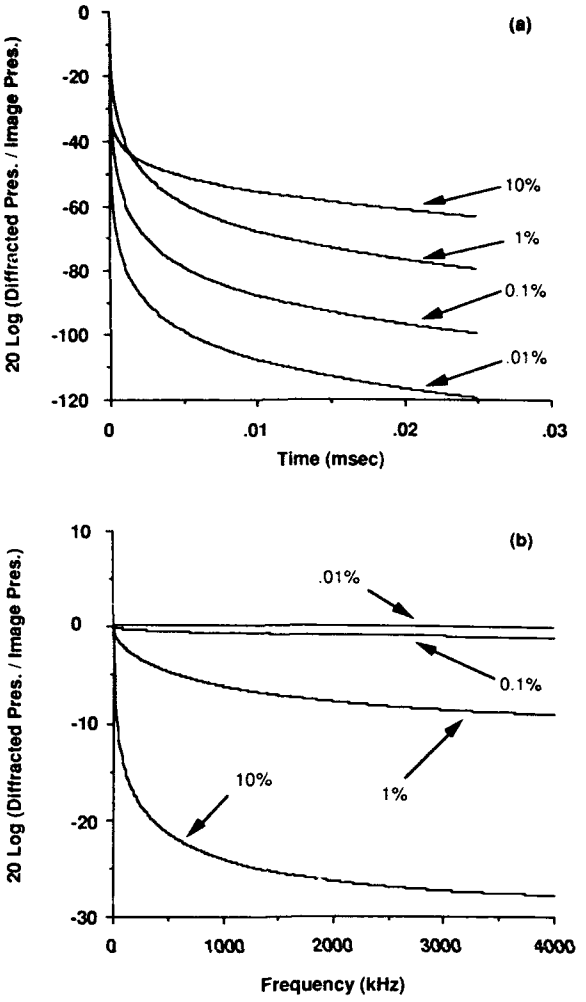

FIG. 4. Diffracted pressure as a function of (a) time and (b) frequency relative to the pressure of an image reflection for several nearly flat wedges.

C. Recipes for the wedge assemblage

In an application of the WA approach to a particular scattering problem, it is useful to regard the "method" as loose framework in which the BT solution is applied to complicated surfaces. Such a definition invites different prescriptions for the generation of the assemblage of wedges. One motivation for considering different recipes is that one may be computationally more efficient than an-

other. On that subject, it should be noted that the overall computational burden may also depend on what one wants to do with the impulse response. For example, a FFT may be performed on the estimated impulse response in order to calculate the scattered complex pressure at discrete frequencies. Another motivation is that a certain measure of the robustness of the WA approach can be demonstrated by the degree to which the results are, in some limiting sense, independent of the particular manner in which the wedge assemblage was generated.

In previous papers on the WA approach, the generation of the assemblage of wedges that was used to approximate the rough surfaces of interest (and hence its impulse response) attempted to get the best estimate for the scattered field from an assemblage defined by a uniform spatial sampling interval (Δx) of the actual surface. For brevity, this sampling scheme will be referred to as SWA (for spatial wedge assemblage). If the impulse response of the complex surface of interest is being calculated at discrete time intervals ($t_i = i^* \Delta t$), then obviously, for the general scattering geometry, this scheme may result in a temporal sampling of the assemblage that is nonuniform. That is, the time separation between any two adjacent wedges in the assemblage may not be constant. In fact, for a fixed Δt and a decreasing Δx, the situation eventually arises in which some neighboring wedges cannot be resolved temporally while for others the time resolution of the calculation is more than adequate. In a sense, such a situation is equivalent to calculating the impulse response of the spatially uniform assemblage of wedges with a time resolution sufficient to resolve all wedges and then passing the resulting time series though a moving average filter whose averaging window varies across the time series in a complicated way.

A new approach to defining the assemblage of wedges is suggested by the observation that the diffracted wave that radiates from a wedge apex is most energetic when it first arrives at the receiver. Thus a more accurate estimate for the impulse response of the rough surface at a particular time t' can be obtained by adding any diffraction from wedges so located on the surface that they first arrive at time t' to the tails of diffractions that have previously arrived. If an estimate of the impulse response of the rough surface is desired at fixed time intervals, this approach (henceforth referred to as temporal wedge assemblage or TWA) will result in an assemblage of wedges that is temporally uniform (i.e., adjacent wedges are separated by ± 1 Δt) but spatially nonuniform (Δx not constant between wedges).

Although a numerical investigation of these two approaches to defining the wedge assemblage is not given here, in all cases where the two were compared the TWA method outperformed the more commonly described SWA recipe. While both methods can be made to agree with each other and usually the benchmark, for the SWA approach convergence to the benchmark usually required more CPU time and user guidance. This was particularly obvious as the frequency increased. For these reasons, all WA calculations shown in this paper were generated from wedge assemblages described by the TWA recipe.

III. THE WA MODELING OF THE BENCHMARK PROBLEM

A. Scattering cross sections

As mentioned earlier, the Biot–Tolstoy solution for the impulse response of a wedge was derived for point sources and receivers. Very often, however, the most convenient benchmark comparisons are for incident plane waves, distant receivers, 1-D surfaces, and usually in the frequency domain. While the particular benchmark solution technique employed in this study is not limited to 1-D surfaces, it certainly is computationally less intensive if restricted to them. Given such practical concerns as computational costs, the approach adopted in this paper is to simulate for the WA calculations (at least over a useful frequency band) this limiting case of incident plane waves and distant receivers. What follows is a discussion aimed at examining (within the context of the BT solution for the diffracted wave) the conditions that must be meet to satisfactorily approximate this scattering scenario.

If the source is a point source, the problem is no longer two dimensional. Let the incident field be given by

$$P_{\text{inc}}(x,z) = \frac{P_0 D(x,z)}{[(x-x_s)^2+y^2+(z-z_s)^2]^{1/2}} \exp[ik((x-x_s)^2 + y^2+(z-z_s)^2)^{1/2}], \tag{13}$$

which has units of force per unit area. Note that P_0 still has units of force per unit length and y_s is taken (without loss of generality) to be zero. Note that the insonification function, $D(x,z)$ is the same as in Eq. (1); it has not been redesigned to attenuate the incident field in the y direction. The total power radiated by this source through the 2-D surface patch is given by

$$\Pi_{\text{inc}} = \frac{P_0^2}{\rho c} \int_{-\infty}^{\infty} \int_{-\infty}^{\infty} \frac{[D(x,z)]^2}{[(x-x_s)^2+y^2+(z-z_s)^2]^{3/2}} \times [-(z-z_s)]\,dx\,dy. \tag{14}$$

Note that now this calculation involves ρ, the density of the three-dimensional fluid. For 2-D surfaces of finite extent, the incident field due to a point source will appear planar across the surface in the xz plane provided $R_S \gg L^2/\lambda$, where R_S is the distance from the source to the center of the scattering patch. If this holds, the power per unit length radiated through the central 1-D slice of the surface can easily obtained simply by setting $y=0$ and performing the integration in Eq. (14) over x from $-\infty$ to $+\infty$. Proceeding as we did earlier for the tapered incident plane-wave source, this quantity can then be used to define an effective intensity (energy per unit time per unit area)

$$I_{\text{inc}}=\frac{P_0^2}{\rho c L \sin\theta_{\text{inc}}}\int_{-\infty}^{\infty}\frac{[D(x,z)]^2}{[(x-x_s)^2+y^2+(z-z_s)^2]^{3/2}}\times[-(z-z_s)]dx=\frac{gP_0^2}{\rho c L R_S^2}\sqrt{\frac{\pi}{2}} \tag{15}$$

and a dimensionless cross section

$$\sigma(\theta_{\text{inc}},\theta_{\text{scat}})=\sqrt{\frac{2}{\pi}}\frac{\rho c R_S^2 R_R I_{\text{scat}}}{gP_0^2}. \tag{16}$$

The equation above reflects the fact that the incident power spreads spherically while the scattered power spreads cylindrically. In the next section, this equation gets modified somewhat based on consideration of the range dependence exhibited by the BT solution.

B. Point source versus line source solutions

Up to now, the infinite extent of the surface in the y direction has been ignored. For the WA calculations, no matter how far the point source is placed from the surface, at some point along the wedge apex the curvature of the incident field is detected. Earlier, definitions for the scattering cross sections that take into account differences in geometric spreading between the two calculations were defined [Eqs. (7) and (16)]. Therefore, what now needs to be determined are the conditions for which the BT solution for the wedge-diffracted wave has the frequency dependence of the wedge-diffracted wave that results when the incident field is due to a distant line source ($kR_S \gg 1$).

It is well known[14] that for a plane-wave source and receiver in the far field ($kR_R \gg 1$), and away from the geometric shadow boundary or reflection direction, the field diffracted by an infinitely long, impenetrable wedge has a frequency dependence that goes like $f^{-1/2}$. To see how the BT solution for the diffracted wave can have this frequency dependence for these geometries, begin with Eq. (9) and express time (t) in terms of the least time τ_0 plus an incremental time τ. Medwin[2] has determined that for $\tau/\tau_0 \ll 1$ the diffracted wave can be approximated (to first order in τ/τ_0) by

$$P_\delta(\tau)=\left(\frac{-S\rho}{4\pi\sqrt{2\theta_w}}\right)\{\beta\}\Omega(r,r_0)\tau^{-1/2}, \tag{17}$$

where

$$\Omega(r,r_0)=(r_0r^2+r_0^2r)^{-1/2} \tag{18}$$

and, for the geometries being discussed, $\{\beta\}$ is now approximately a constant. There are several things to note at this point. Clearly, $\Omega(r,r_0)$ is the geometric spreading term. In order to properly simulate an incident plane wave and a distant receiver this spreading factor must be removed from the diffracted response of each wedge that contributes to the scattered intensity. This suggests that Eq. (16) be rewritten:

$$\sigma(\theta_{\text{inc}},\theta_{\text{scat}})=\sqrt{\frac{2}{\pi}}\frac{\rho c I'_{\text{scat}}}{gP_0^2}, \tag{19}$$

where

$$I'_{\text{scat}}=\frac{1}{\rho c}\left|\sum_{i=1}^{M}P_{\delta_i}\frac{\Omega_{\text{ref}}}{\Omega_i}\right|^2. \tag{20}$$

Here, the sum is over the M wedges of the assemblage. Also, Ω_i is the spreading term and P_{δ_i} is the diffracted pressure at the receiver due to the ith wedge; $\Omega_{\text{ref}}=1(m)^{-3/2}$. Note that if the source is much further away from an apex than the receiver is from that apex ($r_0 \gg r$), then Ω_i reduces to a familiar form that clearly corresponds to spherical spreading from the source and cylindrical spreading from the apex. Finally, note that the only time dependence exhibited in Eq. (17) goes like $t^{-1/2}$ which has a Fourier transform that goes like $f^{-1/2}$. From Eq. (19), a WA estimate of the scattering strength is calculated. This calculation can be compared to the scattering strength derived from Eq. (7) for the benchmark solution technique.

Upon further examination, it is easy to see that the requirement that $\tau/\tau_0 \ll 1$ essentially puts a limit on the maximum wavelength for which Eq. (17) applies. To see this, suppose that $\tau_{\max}$ is a time sufficiently long to include information on the lowest frequency of interest. From the sampling theorem, it is known that this lowest frequency is $f_{\min}=1/\tau_{\max}=c/\lambda_{\max}$. The requirement that $\tau_{\max}/\tau_0 \ll 1$ is, after some algebra (and recall $Z=0$), equivalent to the requirement that

$$\lambda_{\max} \ll r_0+r. \tag{21}$$

For receiver directions way from the geometric shadow boundary or reflection directions, this criterion places a lower frequency limit on the $f^{-1/2}$ behavior of the BT solution. As for receivers is in the direction of the reflection or geometric shadow boundary, it can be noted, that for both the line and point source solutions these geometries lead to frequency-independent responses.

C. Exploiting the periodicity of the surface

Because of the periodicity of the surfaces of interest, the fact that plane waves are involved, and because the single-scatter approximation has been evoked, certain computational short cuts can easily be implemented in the time domain. In brief, one uses the fact that the impulse response from a single period of a sinusoid contains all the information necessary to calculate the impulse response of a sinusoidal surface having any number of periods. Then, simply by calculating the time interval between points on the surface separated by one period and replicating the impulse response due to a single period of the surface at this interval, the impulse response of the extended surface can be calculated. This process eliminates redundant calculations and also serves to weaken the requirements that $R_S \gg L^2/\lambda$ and $R_R \gg L^2/\lambda$ since phase differences between surface points separated by $n\Lambda$ (n an integer, Λ the wavelength of the sinusoid) are eliminated.

IV. BENCHMARK COMPARISONS

In this section, the results of numerical experiments involving different pressure-release sinusoids and scattering

TABLE I. Amplitudes, wavelengths, and maximum slopes for each of three different finite-length sinusoids.

Sinusoid	h (cm)	Λ (cm)	Max. slope (deg)
S1	0.15	4.0	13
S2	0.15	2.0	25
S3	0.30	2.0	43

geometries are considered. This exercise was conducted using three different finite-length sinusoids (labeled S1, S2, S3). The amplitudes and wavelengths for these sinusoids are listed in Table I. Also listed in this table is the maximum slope for each sinusoid. This parameter is of interest because it is related to the onset of geometric shadowing and to the relative importance of multiple scattering. In each numerical experiment considered, the total number of periods for the sinusoids was selected to ensure that $1/kg \sin\theta_s \ll 1$ for the minimum acoustic wave number considered. The source and receiver ranges, which were equal in all cases, were varied in order to satisfy Eq. (21) for the longest acoustic wavelength of interest.

A. Reflectionlike diffractions from small roughness sinusoids

As mentioned earlier, what some have found to be a disturbing aspect of the WA modeling of scattering from rough surfaces is the omission of terms that correspond to reflections from flat patches of the surface of interest. For sinusoidal surfaces, these flat patches have zero area since a tangent plane only "fits" the surface at a point. In another sense, one intuits that reflection should also be the dominant mechanism if the surface roughness becomes very small compared to the acoustic wavelength. Previously in this paper, it was shown that a slightly wedged surface can yield the reflectionlike response associated with an infinite flat surface. In this section, it is shown that reflectionlike results for slightly rough surfaces can be obtained from wedge diffractions.

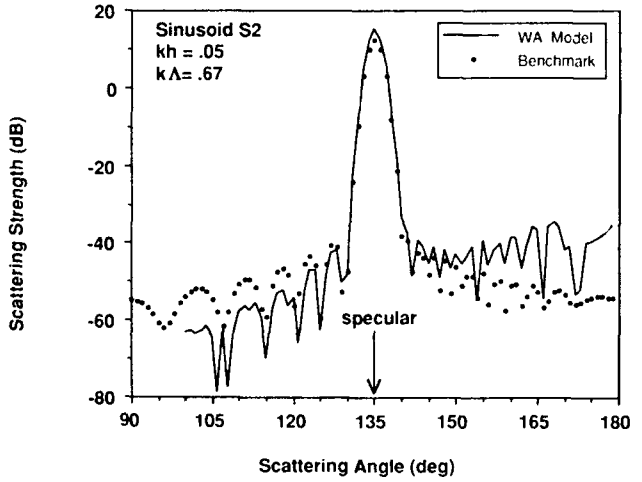

FIG. 5. Comparison of scattering scattering stengths (dB) vs θ_{scat} for 501 periods of the sinusoid defined as S2 in Table I. The grazing angle of incidence is 45 deg and $kh=0.05$.

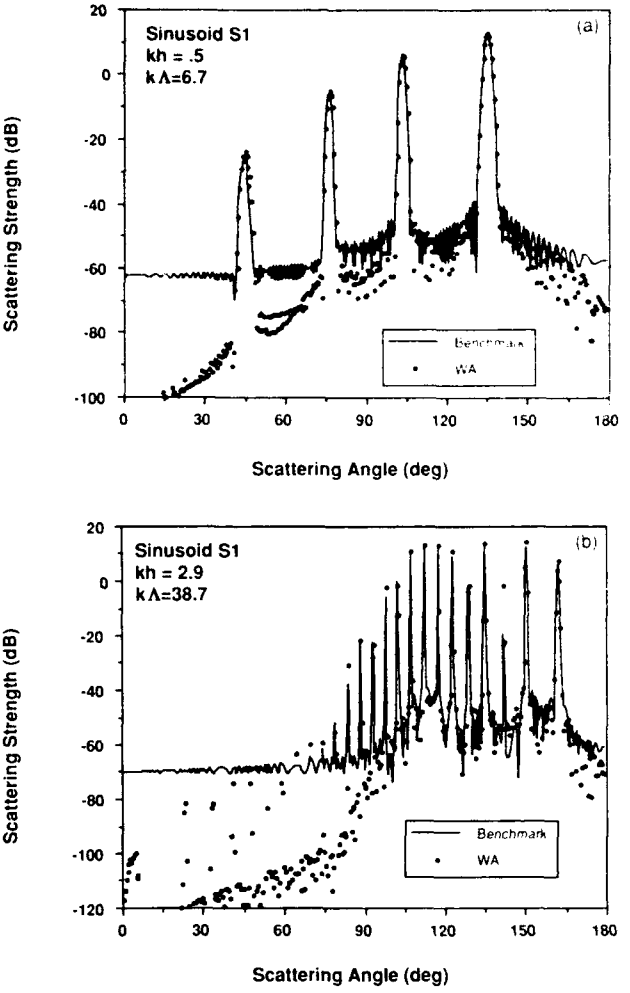

FIG. 6. Comparison of scattering scattering stengths (dB) vs θ_{scat} for 31 periods of the sinusoid defined as S1 in Table I. The grazing angle of incidence is 45 deg. In (a) $kh=0.5$, $k\Lambda=13.3$; in (b) $kh=2.9$, $k\Lambda=77.3$.

Shown in Fig. 5 is the scattering strength plotted versus receiver direction obtained from the diffraction-only WA model for the case of a plane wave incident at 45 deg on a sinusoidal surface (501 periods of S2, $L=10.02$ m). In this case, $kh=0.05$, which is generally considered optically flat. The WA calculation was performed using a time resolution of 2.0E-07; a 2^{15} fast Fourier transform (FFT) was performed on the WA estimate of the impulse response. The source and receiver ranges were set at 10 m from the center of the scattering patch for this test. Also plotted in this figure is the calculation from the benchmark solution. It should be mentioned that the benchmark solution technique required a significantly finer surface discretization ($\Delta x=\lambda/40$ instead of $\Delta x=\lambda/10$) to achieve a stable solution for this case of very small kh. Note the quite good agreement for the beam in the specular direction. This comparison clearly demonstrates that diffractions from a slightly rough finite-length surface can behave like a reflection from a finite-length surface.

On another level, this result taken together with the physics known to be included in the WA model presents a view that is somewhat different from the traditional one in

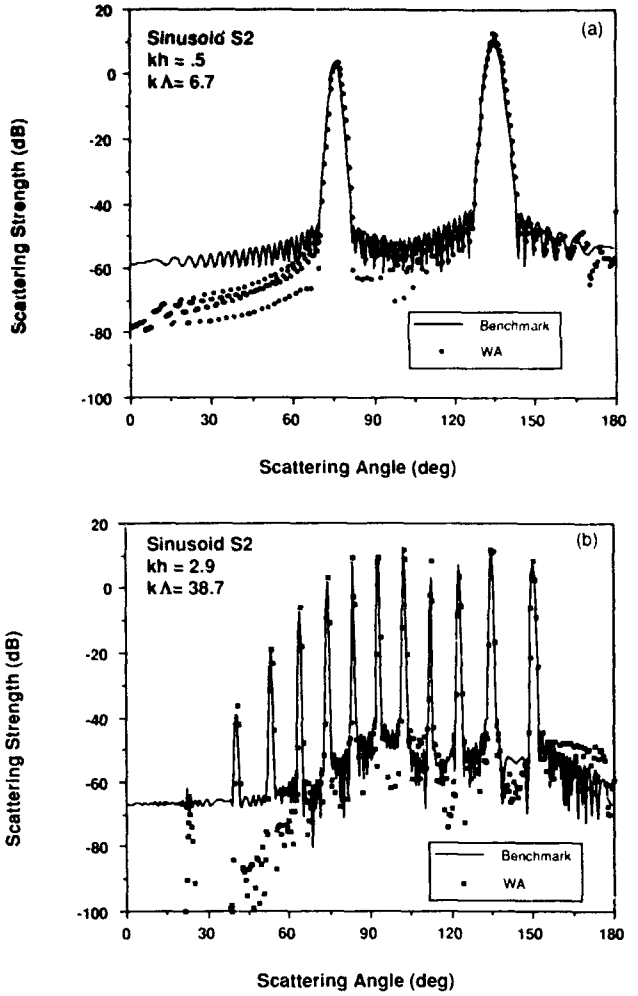

FIG. 7. Comparison of scattering scattering stengths (dB) vs θ_{scat} for 31 periods of the sinusoid defined as S2 in Table I. The grazing angle of incidence is 45 deg. In (a) $kh=0.5$, $k\Lambda=6.7$, in (b) $kh=2.9$, $k\Lambda=38.7$.

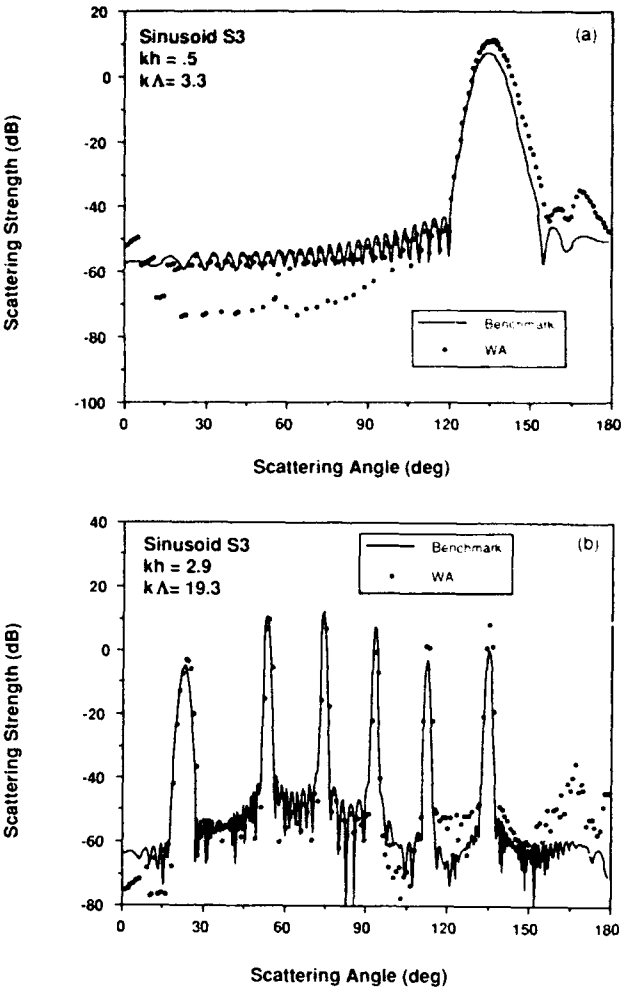

FIG. 8. Comparison of scattering scattering stengths (dB) vs θ_{scat} for 31 periods of the sinusoid defined as S3 in Table I. The grazing angle of incidence is 45 deg. In (a) $kh=0.5$, $k\Lambda=3.3$, in (b) $kh=2.9$, $k\Lambda=19.3$.

which reflection describes the plane-wave scattering when kh gets small. This new view is one in which diffractions from the microroughness describe the scattering right up to the point where the actual roughness (not kh) vanishes. It is only at this point that the reflection begins to exist and takes over in a manner that leads to a smooth transition for the scattered pressure field.

Upon closer inspection, it can be noted that the WA result predicts slightly more energy scattered into the specular direction. Also there are some differences in the level and locations of the side lobes. In the forward direction, the sidelobes for the WA results are significantly higher. Because the major point of this section is clearly made with this comparison, an effort was not undertaken to pin down the exact sources of these differences. However, the following are candidate sources for these discrepancies: First, there may be slight differences in the effect of the taper function in the frequency and time domains. Second, multiple scattering is ignored in the WA calculation as is any sort of shadowing phenomena. These related phenomena probably account for the increase in the sidelobes in the forward direction and possibly, through the lack of destructive interference, the over prediction in the specular direction.

B. Comparisons for higher *kh*, other sinusoids

In this section, comparisons against the benchmark solution are made for the three sinusoids listed in Table I. Two arbitrarily selected values for kh are considered (0.5 and 2.9). Because the combination of Λ and h varies among the sinusoids, the number and locations of the diffracted orders, varies for a fixed kh. The format used is the same as in the previous figure. For all cases in this section the number of periods of the sinusoidal surfaces was 31, the time resolution for the WA calculations was 2.0*e*-07 s, and an FFT of length 8192 was performed to get the frequency response. As in the previous section, the source is incident at 45 deg. The source and receiver are located 1 m from the center of the surface. Shown in Figs. 6–8 are the results for sinusoids S1, S2, and S3, respectively.

Referring in general to all three figures, it is clear that the WA results compare quite well with the benchmark solution in the backscattered direction. Note that in this angular range the WA calculation are able to resolve dif-

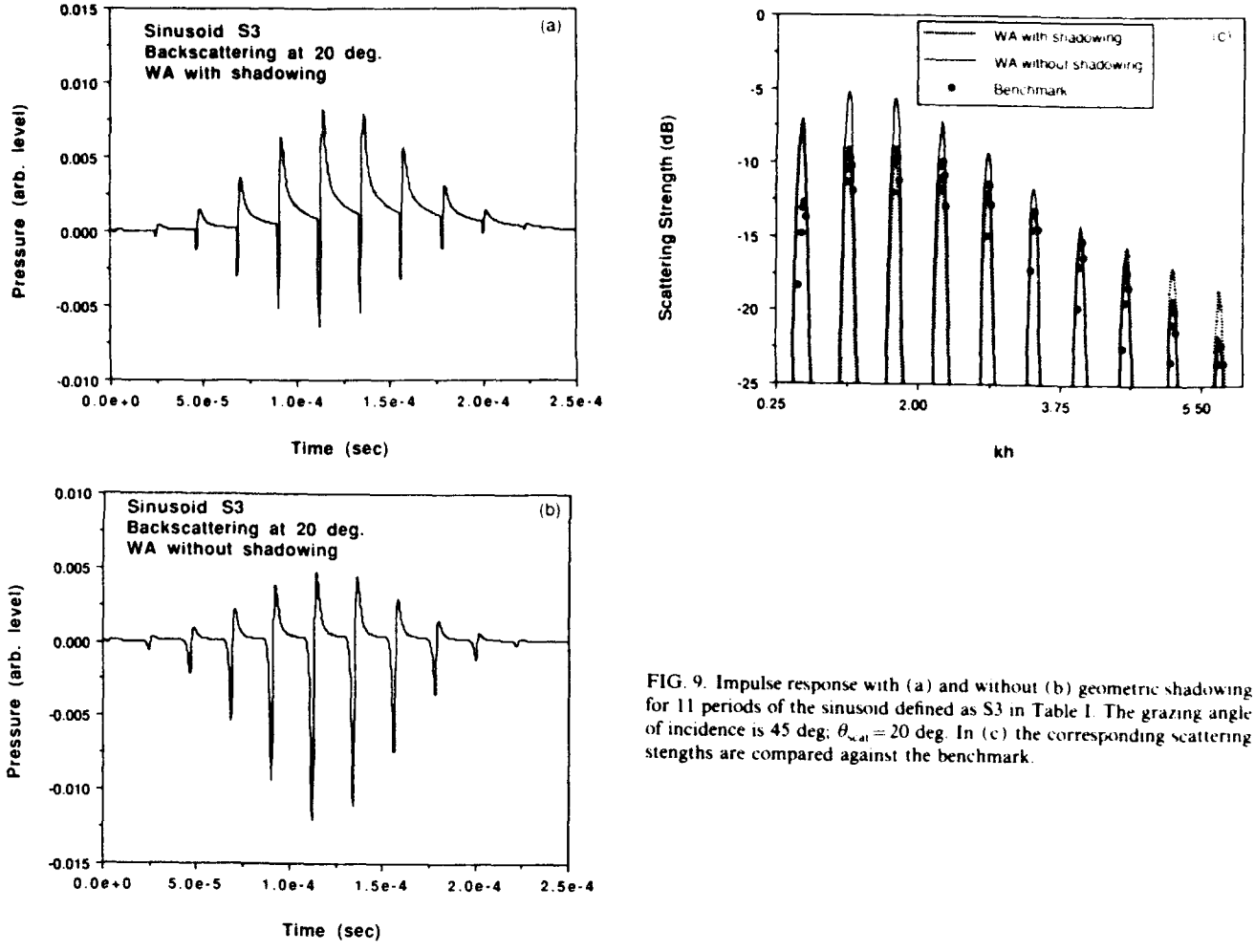

FIG. 9. Impulse response with (a) and without (b) geometric shadowing for 11 periods of the sinusoid defined as S3 in Table I. The grazing angle of incidence is 45 deg; $\theta_{scat} = 20$ deg. In (c) the corresponding scattering stengths are compared against the benchmark.

fracted orders that are hidden below the computational noise floor of the benchmark solution. These diffracted orders appear at precisely the angles predicted by the grating equation. For sinusoids S1 and S2, this high level of agreement with the benchmark extends to the forward direction as well. For S1, at $kh = 2.9$, it can be noted that the WA model overpredicts the scattering in the specular direction. Note that in this case the specular direction is quite suppressed relative to the other diffracted orders. This phenomena is a manifestation of Brewsters reflection anomaly for finite length surfaces. Calculation by the WA model in this direction for the parameters selected are quite sensitive since the time series must be Fourier transformed and then sampled near the nulls of the resulting frequency response.

Returning to the comparison for sinusoid S3 (which it can be noted from Table I has the largest maximum slope), there are significant discrepancies at both values of kh in the forward diffracted orders. For the diffracted orders not in the shadow region of this sinusoid ($43 \text{ deg} < \theta_{scat} < 137$ deg), it is suggested the differences noted are due to the lack of multiple scattering in the WA calculations. Obviously, shadowing cannot affect the scattering into these diffracted orders. For the forward diffracted orders within the angular region where the partial shadowing of the surface from the receiver can occur ($\theta_{scat} > 137$ deg), the lack of shadowing effects in the WA calculations should also be playing a role in the mismatch with the benchmark. The fact that the WA calculations tend to compare well against the benchmark for the backscattered orders suggests that multiple scattering may have a less important role for backscattering.

Generally speaking, there is little that distinguishes the discrepancies in the WA/benchmark comparisons that are clearly multiple scattering related (i.e., in diffracted orders outside the angular region where the shadowing of the surface is a concern) and the discrepancies that may be due to both a lack of shadowing and a lack of multiple scattering in the WA model. In the next section, the effect of including geometric shadowing in these WA calculations is explored further in order to help differentiate between shadowing effects and multiple scattering effects.

C. Geometric shadowing effects in WA modeling

In the WA calculations presented thus far, no attempt has been made to include the effects of the partial shadowing of the receiver. That is, secondary sources located on the surface have been allowed to propagate through any part of the surface that obstructs the path to the receiver. Note, source shadowing need not be discussed since the angle of incidence for the incoming plane wave exceeds the maximum slope of any of the sinusoids. A simple treatment

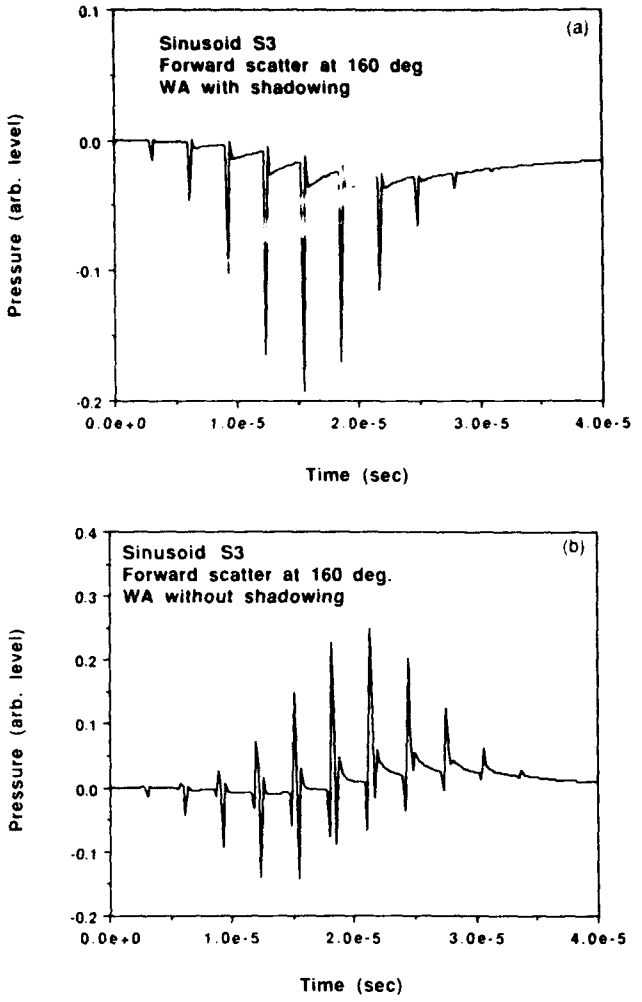

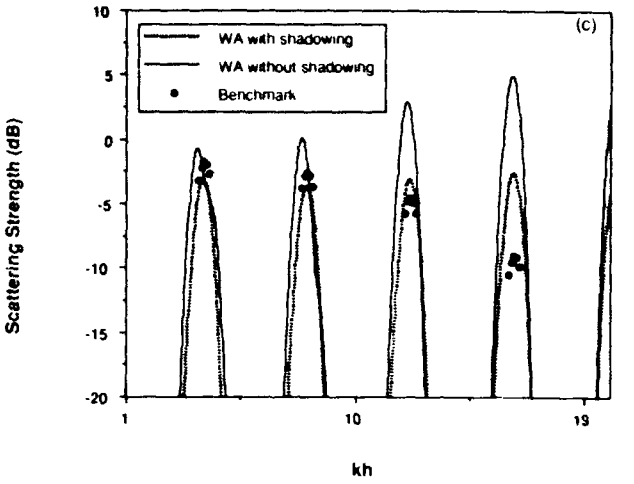

FIG. 10. Impulse response with (a) and without (b) geometric shadowing for 11 periods of the sinusoid defined as S3 in Table I. The grazing angle of incidence is 45 deg; $\theta_{scat} = 160$ deg. In (c) the corresponding scattering stengths are compared against the benchmark.

of the shadowing phenomena is to identify in a geometric sense patches of the surface that are obstructed and simply not include these contributions to the scattered field at the receiver. Within the context of a single scatter approximation this idea is a reasonable one. Indeed, it may be argued that the single scatter approximation requires geometric shadowing since multiple scattering is the only mechanism available to get energy into the shadowed regions of the surface. Obviously, the inclusion of geometric shadowing in the WA model cannot effect the calculation of the energy diffracted into orders that are outside the angular region where shadowing occurs. This fact helps substantiate the earlier suggestion that where the WA departs from the benchmark for these diffracted orders, it is the lack of multiple scattering that is the primary cause.

For testing the effect of geometric shadowing on the WA calculations, it is clear that sinusoid S3 is the best choice for further investigation since it has the steepest maximum slope. Further, it should serve well for this test to consider a single scattering direction that is within the angular range where shadowing occurs and compare the WA calculations made with and without geometric shadowing against the benchmark over a range of frequencies (or kh). Comparisons of this kind are shown in Figs. 9 and 10 for scattering angles of 20 and 160 deg respectively. These scattering directions put the receiver well within this angular region for backward and forward scattering, respectively. Also shown [Figs. 9(a),(b) and 10(a),(b)] are the corresponding impulse responses calculated from the WA model, with and without geometric shadowing.

Consider the backscatter geometry first. From Fig. 9(a) and (b), it is clear that the inclusion of geometric shadowing has the effect of excluding wedge diffractions that have strong negative pressure excursions and, from the relative lack of cancelation, raising the positive excursions. Looking now to the comparison with the benchmark in the frequency domain, it is clear that the change in the impulse response that results from the inclusion of geometric shadowing effects significantly alters the WA results. Basically, what is observed is that the WA result that includes shadowing effects compares more favorably with the benchmark at low kh than does the no-shadowing WA calculation. For higher kh, this trend reverses. The strong mismatch for the first resonance may be related to the short length of the sinusoid (only 11 periods). Clearly, shadowing effects are only part of the phenomena that is missing in the WA calculations. Recall that based on Fig. 8, it was suggested that multiple scattering has a less important role for backscattering than for forward scattering. While this may indeed be generally true for backscattered directions out of the angular region where shadowing is a concern, it is clear from Fig. 9(c) that deep within this

shadow region multiple scattering is also important.

Turning now to the forward scatter geometry (Fig. 10), it can be seen that the impulse response is even more dramatically affected as a result of including shadowing in the WA calculation. In this case, strong wedge diffractions are being excluded from the time series. In the frequency domain comparisons with the benchmark, the shadowing corrections do move the WA calculation in the right direction, however, as kh increases the effect is not enough to bring the WA results in line with the benchmark. Again, it appears that shadowing only partly explains these results. Clearly, a more complete investigation into the role of multiple scattering is warranted. Such an investigation has been planned for future work.

V. CONCLUSIONS

Several conclusions can be stated based on the benchmarking and other numerical experiments conducted in this study. First, it has been shown that a diffraction-only WA scattering model can give excellent results for the problem of plane-wave scattering from pressure-release sinusoidal surfaces over a broad range of kh and $k\Lambda$. It has been shown that this holds even when kh is quite small. An explanation for this result in terms of the behavior of the diffracted wave for nearly flat wedges has been put forth. The principle shortcoming of the WA model has been identified as the lack of multiple scattering effects. However, this is primarily a concern only for quite steep sloped surfaces and then more so for forward scattering then backward scattering. In connection with this result, it has been demonstrated that geometric shadowing does not by itself adequately address the scattering into the shadowed region.

ACKNOWLEDGMENTS

It gives the author great pleasure to acknowledge the many insightful discussions he has had with Dr. Jorge Novarini on the subject of the wedge assemblage method. Also, the author wishes to thank Professor C. S. Clay for his encouragement and his useful comments relating to the preparation of this manuscript. This work has been sponsored by the Office of Naval Research. This document (NRL contribution number NRL/JA/7181-92-0001) has been reviewed and is approved for public release.

[1] H. Medwin "Shadowing by a finite barrier," J. Acoust. Soc. Am. **69**, 1060–1064 (1981).
[2] H. Medwin, E. Childs, and G. M. Jebsen "Impulse studies of double diffraction: A discrete Huygens interpretation," J. Acoust. Soc. Am. **72**, 1005–1013 (1982).
[3] W. A. Kinney, C. S. Clay, and G. A. Sandness, "Scattering from a corrugated surface: Comparison between experiment, Helmholtz-Kirchhoff theory, and the facet-ensemble method," J. Acoust. Soc. Am. **73**, 183–194 (1983).
[4] W. A. Kinney and C. S. Clay, "The spatial coherence of sound scattered from a wind-driven surface: Comparison between experiment, Eckart theory, and Facet-ensemble method," J. Acoust. Soc. Am. **75**, 145–148 (1984).
[5] W. A. Kinney, "The azimuthal dependence of bistatic surface scattering: A comparison between theory and experiment," J. Acoust. Soc. Am. **77**, 1403–1408 (1985).
[6] J. C. Novarini and H. Medwin, "Computer modeling of resonant sound scattering from a periodic assemblage of wedges: Comparison with theories of diffraction gratings," J. Acoust. Soc. Am. **77**, 1754–1759 (1985).
[7] H. Medwin and J. C. Novarini, "Backscattering strength and the range dependence of sound scattered by the ocean surface," J. Acoust. Soc. Am. 108–111 (1981).
[8] R. R. Lentz, "A numerical study of electromagnetic scattering from ocean-like surfaces," Radio Sci. **9**, 1139–1146 (1974).
[9] R. M. Axline and A. K. Fung, "Numerical computations of scattering from perfectly conducting random surfaces," IEEE Trans. Antennas Propag. **AP-26**, 482–488 (1978);**AP-28**, 949 (1980).
[10] E. I. Thorsos, "The validity of the Kirchhoff approximation for rough surface scattering using a Gaussian roughness spectrum," J. Acoust. Soc. Am. **83**, 78–92 (1988).
[11] E. I. Thorsos and D. R. Jackson, "The validity of the perturbation approximation for rough surface scattering using a Gaussian roughness spectrum," J. Acoust. Soc. Am. **86**, 261–277 (1989).
[12] R. S. Keiffer and J. C. Novarini, "A wedge assemblage method for 3-D acoustic scattering from sea surfaces: Comparison with a Helmholtz-Kirchhoff Method," in *Computational Acoustics*, edited by D. Lee, A. Cakmak, and R. Vichnevetsky (Elsevier, Amsterdam, 1990), Vol. 1, pp. 67–81.
[13] M. A. Biot and I. Tolstoy, "Formulation of wave propagation in infinite media by normal coordinates with application to diffraction," J. Acoust. Soc. Am. **29**, 381–391 (1957).
[14] A. D. Pierce, *Acoustics, An Introduction to Its Physical Principles and Applications* (McGraw-Hill, New York, 1981), pp. 491–494.